Draft version August 5, 2019
Typeset using LaTeX default style in AASTeX62

The Mega-MUSCLES Spectral Energy Distribution Of TRAPPIST-1

David J. Wilson,[1] Cynthia S. Froning,[1] Kevin France,[2] Allison Youngblood,[3,*] Girish M. Duvvuri,[4] P. Christian Schneider,[5] Adam Kowalski,[2,6,7] R. O. Parke Loyd,[8] Alexander Brown, Zachory Berta-Thompson, J. Sebastian Pineda, Jeffrey Linsky,[9] Sarah Rugheimer,[10] and Yamila Miguel[11]

[1] *McDonald Observatory, University of Texas at Austin, Austin, TX 78712*
[2] *Laboratory for Atmospheric and Space Physics, University of Colorado, 600 UCB, Boulder, CO 80309*
[3] *Goddard Space Flight Center, Greenbelt, MD 20771*
[4] *Department of Astrophysical and Planetary Sciences, University of Colorado, Boulder, CO 80309, USA*
[5] *Hamburger Sternwarte, Gojenbergsweg 112, 21029 Hamburg*
[6] *Department of Astrophysical and Space Astronomy, University of Colorado, 389 UCB, Boulder, CO 80309*
[7] *National Solar Observatory, University of Colorado at Boulder, 3665 Discovery Drive, Boulder, CO 80303*
[8] *School of Earth and Space Exploration, Arizona State University, Tempe, AZ 85287*
[9] *University of Colorado, Boulder, CO 80309*
[10] *University of Oxford, Clarendon Laboratory, AOPP, Sherrington Road, Oxford, OX1 3PU, UK*
[11] *Leiden Observatory, P.O. Box 9500, 2300 RA Leiden, The Netherlands*

(Received January 1, 2018; Revised January 7, 2018; Accepted August 5, 2019)

Submitted to ApJ

ABSTRACT

We present a panchromatic Spectral Energy Distribution (SED) of the M8 star TRAPPIST-1, obtained as part of the Mega-MUSCLES Treasury Survey. The SED combines ultraviolet and blue-optical spectroscopy obtained with the *Hubble Space Telescope*, X-ray spectroscopy obtained with *XMM-Newton*, and models of the stellar photosphere and corona. A new Differential Emission Measure model of the unobservable extreme-ultraviolet spectrum is provided, improving on the Lyman α–EUV relations used by the original MUSCLES program. We describe the observations and models used, as well as the recipe for combining them into an SED. We also provide a semi-empirical model SED based on our observations for use in atmospheric modelling of the TRAPPIST-1 planets. **and some science**

1. INTRODUCTION

Among the thousands of planetary systems that have been discovered over the past two and a half decades, TRAPPIST-1 is a standout case. Discovered by the TRansiting Planets and PlanestIsimals Small Telescope (TRAPPIST) survey in 2015 (Gillon et al. 2016), the system is comprised of an M8 ultracool dwarf star orbited by seven planets, all of which have similar masses and radii to Earth and Venus (Gillon et al. 2017; Wang et al. 2017). The planets are almost exactly coplanar, have orbital periods ranging between 1.5 and 18.8 days, and are all in a orbital resonance with at least one other planet (Luger et al. 2017). The system presents a challenging but achievable target for transit spectroscopy observations of the planets, both now with the *Hubble Space Telescope* (HST, de Wit et al. 2016) and in the future with the *James Webb Space Telescope* (JWST, Barstow & Irwin 2016). Beween three and four of the planets orbit at distances where the instellation is such that liquid water might persist on their surfaces. The TRAPPIST-1 system therefore offers opportunities for comparative planetology to test models of planetary habitability, biosignatures and even, given the small orbital separations between the planets, panspermia (Veras et al. 2018).

Corresponding author: David J. Wilson
djwilson394gmail.com

* NASA Postdoctoral Program Fellow

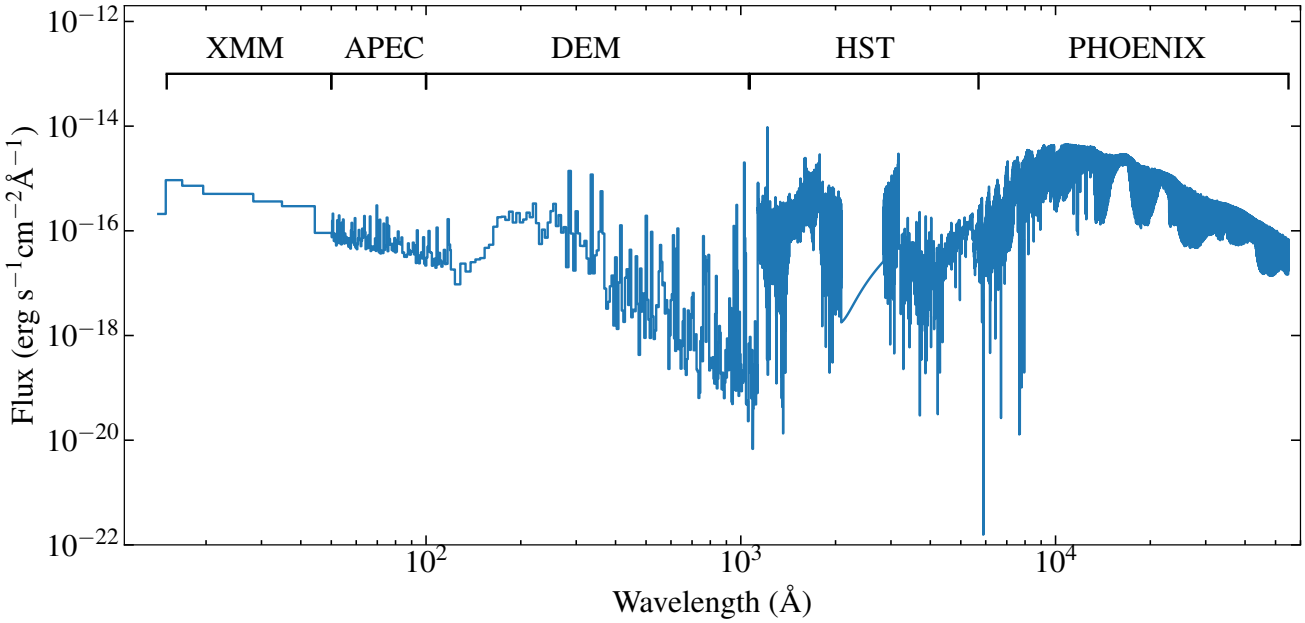

Figure 1. SED of TRAPPIST-1 with all data and models at native resolutions. The sources for each section of the spectrum are labeled above it.

A complete evaluation of the potential habitability of the TRAPPIST-1 planets requires comprehensive knowledge of the parent star. This has proven challenging, with uncertainties remaining over, for example, the star's age (Burgasser & Mamajek 2017), activity (Vidal et al. 1973), and rotation period (Roettenbacher & Kane 2017). Of particular importance, given the the close proximity of the planets to the star, is the X-ray and ultraviolet emission and activity. High-energy radiation can influence the retention and chemistry of planetary atmospheres as well as surface survival conditions O'Malley-James & Kaltenegger (2017). However TRAPPIST-1 is extremely faint at short wavelengths, making detailed characterisation of the high-energy environment in the system challenging. Wheatley et al. (2017) observed TRAPPIST-1 with *XMM-Newton*(XMM), finding variable X-ray luminosity with intensity similar to the modern quiescent Sun. The planets would therefore experience XUV intensities much higher than the Earth, sufficient to significantly alter their atmospheres and strip away surface water. Bourrier et al. (2017a,b) obtained time series observations of the 1215.67Å Lyman α hydrogen emission line, finding that it evolved over a three-month timescale but with no evidence for water escape from TRAPPIST-1c, which transited during their observations. Peacock et al. (2019) used the PHOENIX stellar atmosphere code to model the chromosphere of TRAPPIST-1, scaling it to the Bourrier et al. (2017a)Lyman α measurement and to *GALEX* observations of stars with a similar spectral type, finding that the extreme ultraviolet (EUV) flux varies by an order of magnitude depending on which calibrator was used.

Mega-MUSCLES (Measurements of the Ultraviolet Spectral Characteristics of Low-Mass Exoplanetary Systems) is an HST Treasury program obtaining panchromatic (5 Å–5 μm) spectral energy distributions (SED) of a representative sample of 13 M dwarfs, covering a wide range of stellar mass, age, and planetary system architecture and extending the previous 11-star MUSCLES program (France et al. 2016; Loyd et al. 2016) to stars with lower masses, higher activity and/or faster rotation rates. Here we present the Mega-MUSCLES SED of TRAPPIST-1 (Figure 1), comprised of ultraviolet and x-ray spectroscopy with *Hubble Space Telescope* (HST) and XMM, along with state-of-the-art model spectra. We discuss the improvements made to the data products compared with the MUSCLES program and **do some science**

2. OBSERVATIONS

We observed TRAPPIST-1 with the Cosmic Origins Spectrograph (COS) and the Space Telescope Imaging Spectrograph (STIS) onboard HST on 2017 December 15 and 2018 December 08–12, for a total exposure time of 34781 s.

The COS gratings used were G160M (7010 s), G130M (12404 s)[1] and G230L (2731 s), and the STIS gratings were G430L (1795 s) and G140M (10841 s). Combined, these spectra cover the wavelength range 1130–5700 Å except for a gap between 2080–2840 Å which is not covered by the COS NUV detector. With the exception of the STIS/G430L exposure the observations were obtained using photon counters in TIME-TAG mode. We extracted lightcurves from each spectrum to search for and potentially remove contributions from flares or other stellar activity, but found no significant variation.

For the COS G160M and G130M observations, variations in targets position in the aperture between each orbit induce slight differences in wavelength calibration. To remove this affect we cross-correlated known emission lines in each x1d spectrum to shift each spectrum onto a single wavelength scale before coadding. Doing so provides a small increase in S/N and resolution compared with the x1dsum files produced by the CALCOS pipeline.

In addition to the new observations presented here, TRAPPIST-1 has already been observed multiple times with HST/STIS using the G140M grating covering the Lyman α hydrogen line (Bourrier et al. 2017a,b). We retrieved the data from MAST and combined them, along with our new G140M spectra, to produce a final spectrum covering 1195–1249Å with a total exposure time of 168634 s ($\sim$1.95 d). The automated reduction failed to identify the spectral trace, so we used the flt images to visually identify the spectrum in each exposure, before re-extracting the spectrum with the STISTOOLS x1d routine, fixing the "a2center" keyword to the identified spectrum position. Bourrier et al. (2017b) found that the choice of background region affected the strength of the spectra in some cases, so we experimented with varying the background region for each spectrum. We found that, whilst the signal in some of the individual spectra was altered, the effects on the overall coadd were small. As for the purposes of this paper we are not interested in epoch to epoch changes in the Lyman α line, we kept the default background region for each spectrum in our final extraction.

TRAPPIST-1 has also been observed with the STIS/G140L grating covering 1119–1716Å(Wheatley et al. 2017), but no significant signal was detected. We therefore did not include these data in our analysis.

We further observed TRAPPIST-1 with *XMM-Newton* (XMM) with the thin filters for 23 ks on 2018 December 10, overlapping in time with the COS G130M observations. TRAPPIST-1 was detected with an average count rate of 0.003 c s^{-1}, approximately an order of magnitude lower than that found by Wheatley et al. (2017). Analysis of all available archival data suggested that the Wheatley et al. (2017) result was dominated by a strong flare(s), thus we take our observation to represent the "typcial" X-ray flux.

3. SED

For the most part, the SED was generated following the same procedure as for the MUSCLES SEDs as described by Loyd et al. (2016). Figure 1 shows the full SED and the wavelength ranges covered by the different observational and model sources. Factors unique to TRAPPIST-1 as well as departures from the MUSCLES techniques are described below.

3.1. *X-ray*

The XMM spectrum was fit using the XSPEC package (Arnaud 1996) with models generated using the Astrophysical Plasma Emission Code (APEC, Smith et al. 2001). The data was best fit by a two-temperature model (kT = 0.2, 0.4) and a metalicticy of 0.4 Solar. The model was then used to correct the data at lower energies for instrumental effects to produce the final X-ray spectrum used in the SED, covering the wavelength range of 14-50Å. The integrated observed flux over the energy range 0.1-10 keV was 1.9242×10^{-14} erg s^{-1} cm^{-2}. The APEC model extents beyond the wavelength range covered by the data to 120Åand we inculde that extension in the final SED.

3.2. *Extreme-Ultraviolet and DEM modelling*

The most significant departure from the MUSCLES procedure is the replacement of the Linsky et al. (2014) Extreme-Ultraviolet (EUV) regions with a differential emission measurement (DEM) model, which estimates the coronal emission based on the strength of the detected lines in the FUV spectrum. A model spectrum is required as the region spanning 100–1100 Å is unobservable, both physically due to absorption from interstellar hydrogen between 400-900 Å, and a lack of currently operating instruments at other wavelengths (HST/COS does have some modes that extend down to

[1] One of the planned G130M orbits was not obtained due to late target acquisition. The observation has been rescheduled and the data will be added to the HLSP TRAPPIST-1 spectrum when it is obtained, providing a moderate increase in S/N.

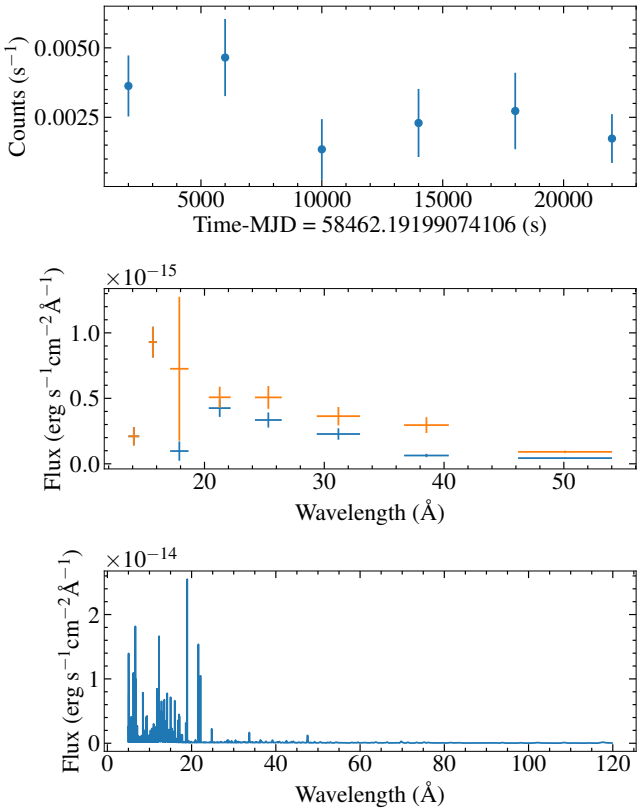

Figure 2. Top: X-ray lightcurve of TRAPPIST-1. Middle: XMM spectrum of TRAPPIST-1. The extracted flux is shown in blue and the model-corrected flux in orange. Bottom: APEC model used to correct the TRAPPIST-1 spectrum. **Model extension to SED?**

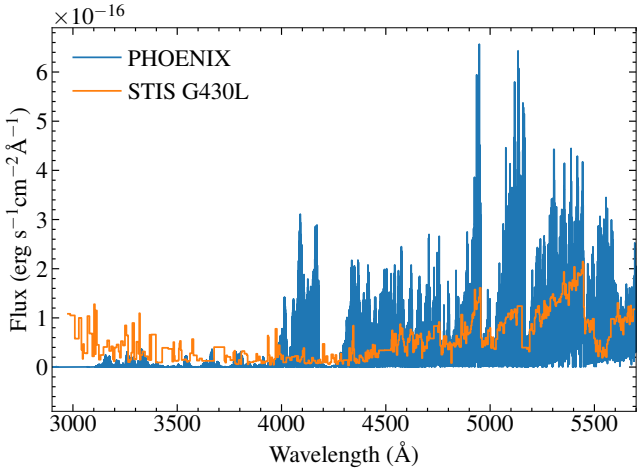

Figure 3. STIS G430L spectrum (orange) used to scale the arbitrary flux of the PHOENIX model (blue). Note the lack of agreement at short wavelengths as coronal/choromosphere flux begins to contribute to the STIS spectrum (see text).

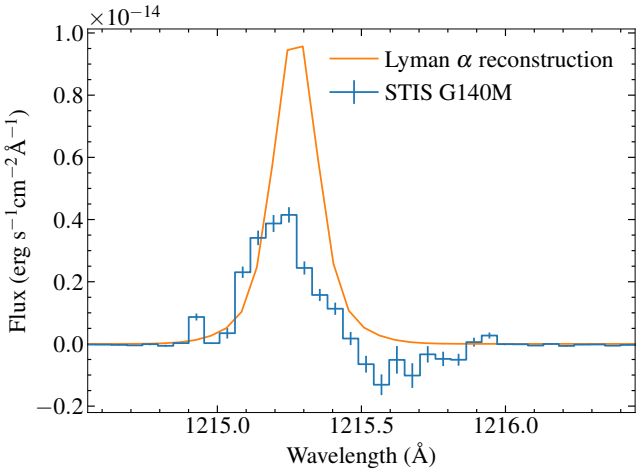

Figure 4. Section of the coadded STIS G140M spectrum showing the H I 1215.67Å Lyman α line, along with a model reconstruction accounting for the loss of much of the flux to interstellar absorption and terrestrial airglow.

900 Å, but these were not sensitive enough to be practical for this program). The DEM model is described in detail in Section 4.

3.3. *Far- and Near- Ultraviolet*

The H I 1215.67 Å Lyman α line is clearly visible in our coadded STIS G140M spectrum, but is heavily affected by both interstellar absorption and terrestrial airglow. We reconstructed the full Lyman α profile via techniques described in Youngblood et al. (2016). Figure 4 shows the spectrum and reconstructed line profile. We found an integrated flux of $F_{\mathrm{Ly}\alpha} = (2.12^{+0.84}_{-0.44}) \times 10^{15}\,\mathrm{erg\,s^{-1}\,cm^{-2}}$, lower but within $2\,\sigma$ of the flux found by Bourrier et al. (2017a). Bourrier et al. (2017b) demonstrated that the Lyman α flux is variable so a small difference is unsurprising. Investigating the time-dependence of the Lyman α flux is beyond the scope of this paper **and will possibly be done by someone else before this gets published**, so we treat our reconstructed line profile as the time-averaged flux.

The COS FUV spectrum was contaminated by airglow from Lyman α and O I over the wavelength ranges 1214–1217Å and 1301–1307Å respectively. Both ranges were removed and replaced by the reconstructed Lyman α profile in the first case and by a polynomial fit to the spectrum on either side in the second.

The COS NUV observations covered the wavelength ranges 1700–2100 Å and 2800–3200 Å leaving a 700 Å gap. This gap is partially covered by a second order spectrum spanning 1950–2150 Å, but the signal was so poor that we chose not to include it. The gap was filled with a polynomial fit to the two wavelength regions, with the range 2790–2805 Å masked out to remove contributions from the Mg II 2800 Å lines.

3.4. *Optical to infrared*

We were unable to obtain ground-based spectroscopy of TRAPPIST-1 contemporaneous with our HST and XMM observations, so wavelengths covering 5700Å–5.55 μ are filled in using a PHOENIX model spectrum from the Göttingen Spectral Library[2](Husser et al. 2013). Using the properties of TRAPPIST-1 gathered by Burgasser & Mamajek (2017) we obtained models with log g = 5.0, Fe/H = 0, α/M = 0 and interpolated a spectrum with $T_{\mathrm{eff}} = 2560$ K. The model flux is arbitrarily scaled, so we fitted it to the STIS G430L spectrum in the region 4500–5696Å. G430L observations in the MUSCLES program were affected by slit losses so an absolute flux calibration could not be guaranteed, necessitating a fit to archival photometry (Loyd et al. 2016). For the Mega-MUSCLES G430L observations we doubled the slit width to 2", ensuring a good flux calibration and allowing us to scale the model directly to the spectrum using a least-squares fit (Figure 3). The blue end of the G430L spectrum contains contribution from the corona that is not included in the PHOENIX model, and thus could affect the scaling. To account for this, we calculated the scaling factor with increasing lengths of the blue end of the G430L spectrum excluded. A clear discontinuity was seen when flux bluewards

[2] http://phoenix.astro.physik.uni-goettingen.de

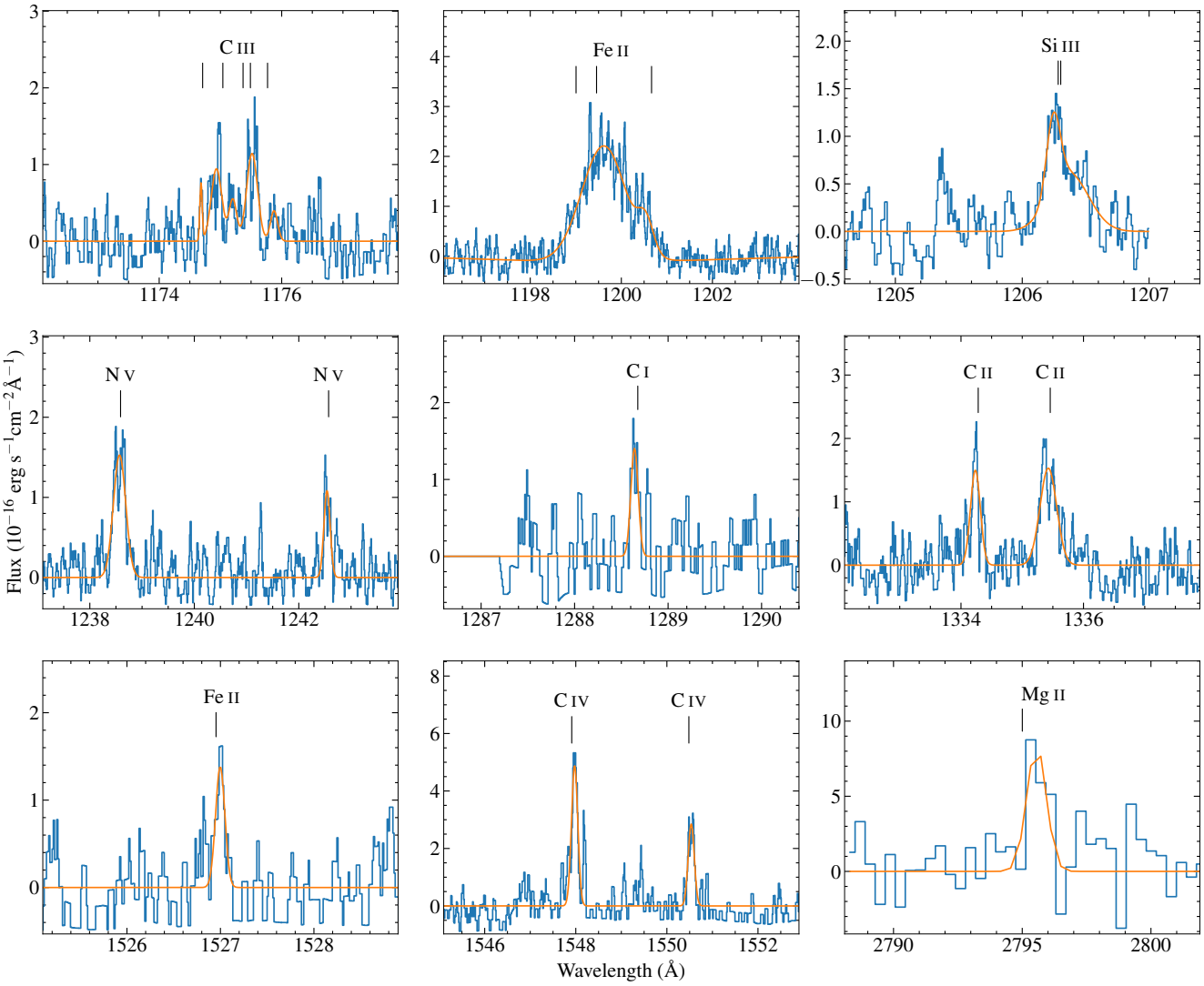

Figure 5. Detected emission lines in COS spectra of TRAPPIST-1 (blue) and the fit used to measure the integrated fluxes (orange). The spectra were smoothed with a 5-point boxcar for clarity, with the exception of the region around the Mg II lines. Line positions were taken from NIST and shifted by the $-56.3\,\mathrm{km\,s^{-1}}$ radial velocity of TRAPPIST-1 Reiners & Basri (2009).

of 4200Å was excluded, with all further cuts consistent to within ≈ 1 per cent. We therefore took the average scaling factor calculated using sections of the G140L spectrum with blue ends ranging between 4200 Å and 5400 Å in 100 Å steps.

4. DIFFERENTIAL EMISSION MEASURE

4.1. *Emission lines*

Multiple emission lines of C, N, Mg, Si and Fe are detected in our COS and STIS spectra (Figure 5). The integrated flux of each line (Table 1) was calculated in the following manner. First, the NIST atomic lines database[3] was searched for any lines that could be contributing to a given emission feature. The spectrum was then fitted with a compound Gaussian model built out of the line list using the ASTROPY SLSQPLSQFitter routine (orange line in Figure 5). The flux was integrated between the zero-intensity points of the model. Errors were estimated by taking the average of the integrated flux of two $\approx$1 Å wide regions near each line, scaled to the range over which the line was integrated.

[3] https://physics.nist.gov/PhysRefData/ASD/lines_form.html

Species	λ_{rest} (Å)	Flux (10^{-18} erg s^{-1} cm^{-2})
C III	1175.5	64.0 ± 7.8
Fe II	1200.0	279 ± 24
Si III	1206.53	34.6 ± 10
N V	1238.821	45.3 ± 4.1
N V	1242.804	16.2 ± 2.8
C I	1288.918	13.8 ± 2.8
C II	1334.532	30.0 ± 0.8
C II	1335.708	52.3 ± 1.3
Fe II	1527.3	17.2 ± 4.0
C IV	1548.202	85.0 ± 5.0
C IV	1550.774	47.8 ± 12.9
Mg II	2796.35	788 ± 81

Table 1. Integrated fluxes for detected ultraviolet emission lines.

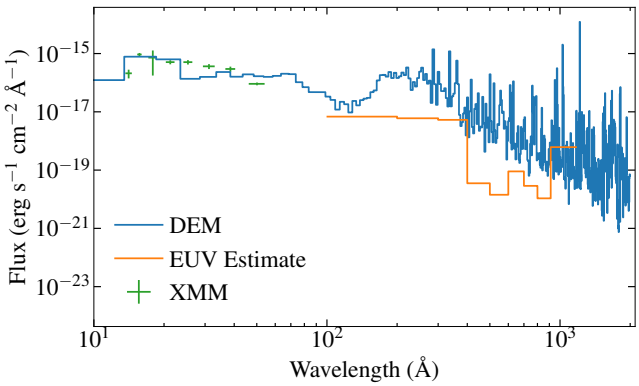

Figure 6. Comparison of the DEM model with the EUV/Lyman α relationships of Linsky et al. (2014), and the XMM spectrum. **add more when dem section finished**

4.2. *Differential Emission Measure*

to be completed by Girish The emission lines detected in the FUV spectrum allow us to model the TRAPPIST-1 coronal emission using a Differential Emission Measure (DEM), filling in the unobservable EUV region of the EUV. The techniques is based on those used by Louden et al. (2017) to reconstruct the high-energy irradiation of an evaporating exoplanet, although our routine has some differences.

The intrinsic specific intensity of a single emission line is:

$$I_{\lambda_{ul}} = \frac{1}{4\pi} \int_{\mathrm{Line-of-sight}} n_u A_{ul} \frac{hc}{\lambda_{ul}} ds$$

where ul indicates a transition from an upper state u to a lower state l, λ_{ul} is the wavelength of the transition, n_u is the number density of the emitting species in the upper state, and A_{ul} is the Einstein rate coefficient of the transition. By rewriting n_u:

$$n_u = \frac{n_u}{n_{\mathrm{ion}}} \frac{n_{\mathrm{ion}}}{n_{\mathrm{el}}} \frac{n_{\mathrm{el}}}{n_H} n_H$$

where n_{el} is the number density of the element of the species, we can construct a contribution function $G(T)$ that depends only on atomic data like the rate coefficient and transition wavelength, the ionization fraction, and elemental abundance. This allows us to rewrite the intensity integral to be:

$$I_{\lambda_{ul}} = \int_{\mathrm{T}} G(T) \Psi(T) dT$$

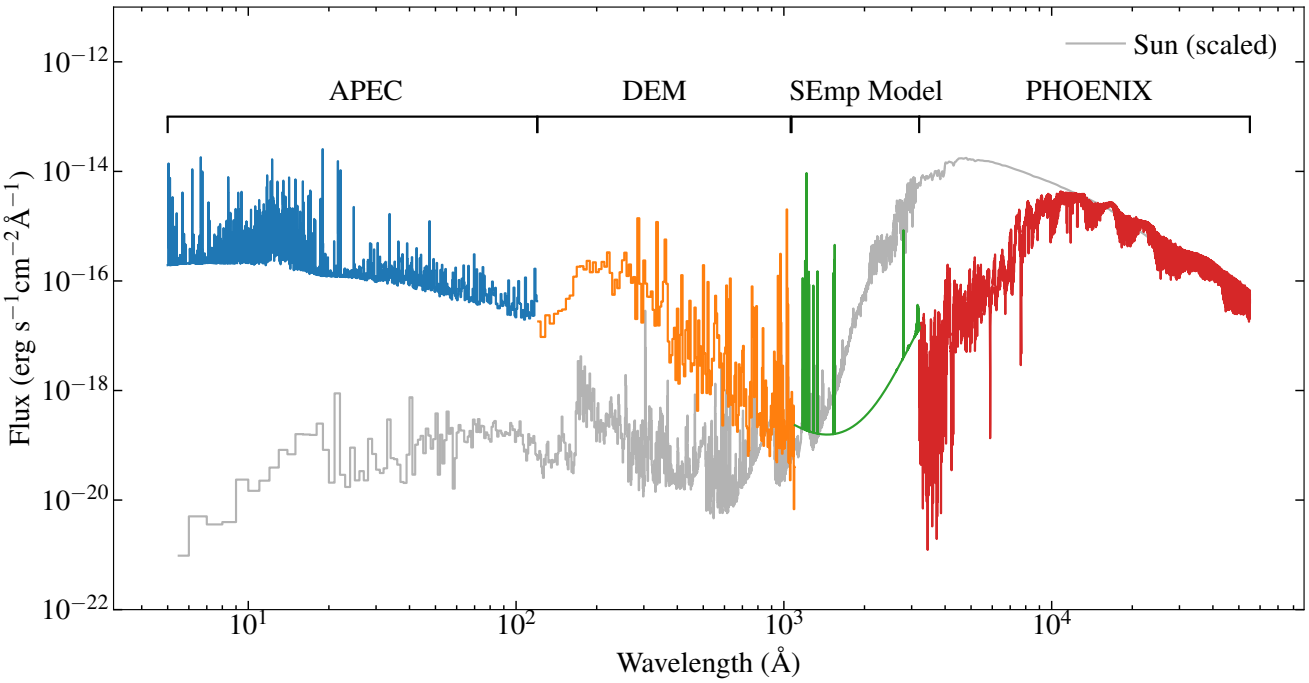

Figure 7. Semi-empirical model spectrum of Trappist-1. The four different models components used are labeled above the spectrum. The spectrum is compared with the quiet Solar spectrum Woods et al. (2009), scaled to have the same blackbody photospheric flux as TRAPPIST-1. The PHOENIX model in the plot has been rebinned to 1 Å for clarity.

where $\Psi(T) = n_e n_H \frac{ds}{dT}$ = the differential emission measure. $G(T)$ measures the contribution of material at a given temperature to the emitted intensity of a line while $\Psi(T)$ measures the amount of material that is present at a given temperature along the line of sight.

We have measured line intensities across a range of formation temperatures , allowing us to fit for Ψ (assuming a continuous function, in this case a 4^{th} order polynomial in loglogspace), and then calculate the expected intensities of lines across the entire wavelength range for which we expect this distribution to apply (i.e. the corona).

5. SEMI-EMPIRICAL MODEL

Given the unavoidable low signal-to-noise of ultraviolet observations of M-dwarfs in general and TRAPPIST-1 in particular, the Mega-MUSCLES data products will also include semi-empirical models constructed from the data, which may be of more utility for model atmosphere studies. The semi-empirical model for TRAPPIST-1 is shown in Figure 7. Four models are used, including the APEC, DEM and PHOENIX models already discussed. The fourth model replaces the COS FUV and NUV spectra covering 1100–3200ÅṪhe model is constructed by first fitting a polynomial to the DEM model and the blue end ($\lambda < 4000$) of the STIS G430L spectrum to create a baseline continuum . Note that this does not represent chromospheric/coronal blackbody continuum emission, but rather the average flux from a forest of weak emission lines. We then added the reconstructed Lyman α line and the fits to the emission lines shown in Figure 5, as well as the PHOENIX spectrum at those wavelengths, to produce the final spectrum section.

Figure 7 compares our final semi-emperical model SED with the quiet Solar spectrum (Woods et al. 2009), which has been scaled to have the same photospheric flux as Trappist-1. The comparison clearly demonstrates the relative difference in high-energy flux between TRAPPIST-1 and the Sun, implying that any planet receiving the same insolation from TRAPPIST-1 as (for example) the Earth receives from the Sun, is experiencing a much higher flux at high-energy wavelengths.

6. DISCUSSION

6.1. *Comparison with model spectra*

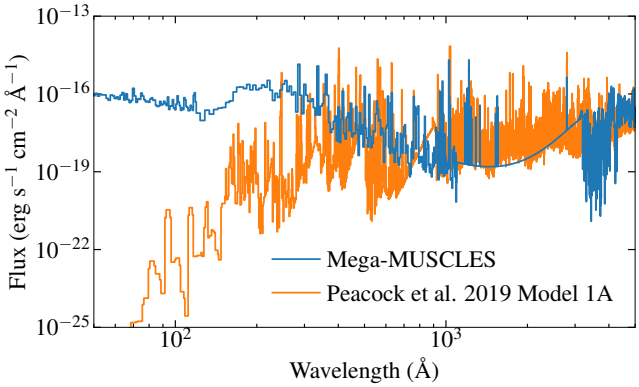

Figure 8. Comparison of the ultraviolet ranges of the Mega-MUSCLES semi-empirical model with the Lyman α-calibrated PHOENIX model 1A from Peacock et al. (2019), binned to 1 Å and scaled to have the same integrated flux at $\lambda > 4000$. Models 2A and 2B are not shown to avoid cluttering the plot, but follow the same overall trends.

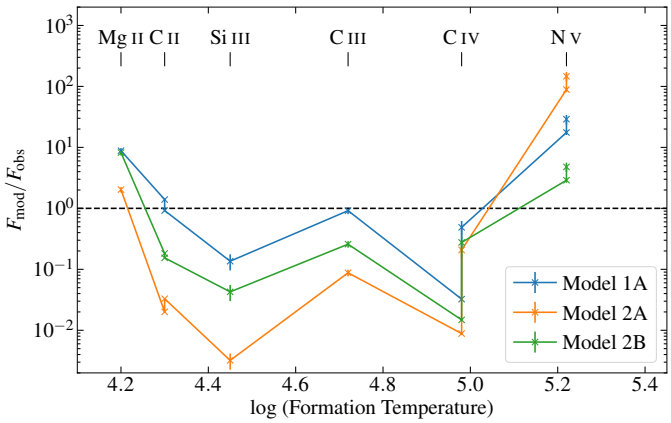

Figure 9. Comparison of the integrated flux of detected emission lines with predicted fluxes measured from the Peacock et al. (2019) models.

Peacock et al. (2019) extended the PHOENIX stellar atmosphere code into the ultraviolet, providing model SEDs of the TRAPPIST-1 chromosphere against which we can compare out observations. The three Phoenix models were calibrated to the Bourrier et al. (2017a) Lyman α flux (1A) and distance-adjusted GALEX photomety of stars with similar spectral types (2A, 2B). Figure 8 shows the X-ray and ultraviolet ranges of the PHOENIX model 1A compared with our semi-empirical model. In the FUV and NUV the two SEDs are in reasonably good agreement, but in the EUV the PHOENIX model underpredicts the flux by multiple orders of magnitude. Future inclusion of the corona in the PHOENIX models may rectify this discrepancy.

Figure 9 compares the integrated fluxes of emission lines detected in our spectrum with the three PHOENIX models as a function of formation temperature. The PHOENIX line strength were measured over the same wavelength ranges used for the COS lines. Excepting the N V lines, which originate in the corona and are therefore not yet fully modelled in the PHOENIX treatment, we find reasonably good agreement between the measured lines and the Lyman α-scaled model 1A, and poorer agreement with the other two models.

MORE SCIENCE HERE!

7. HIGH-LEVEL SCIENCE PRODUCTS

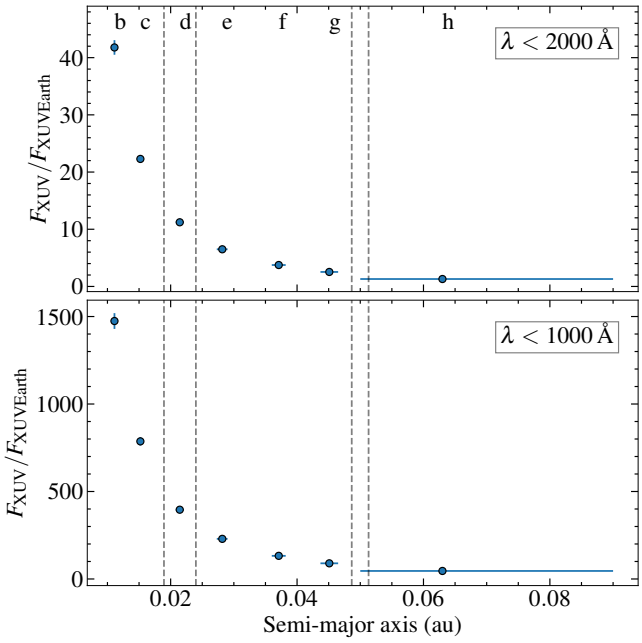

Figure 10. X-ray and UV radiation, defined as all flux at $\lambda < 2000$Å (top) and < 1000Å (bottom), experienced by each of the TRAPPIST-1 planets relative to the Earth. The dotted lines show potential edges of the temperate zone as modelled by Kopparapu et al. (2014).

The TRAPPIST-1 SED will be made available at or before publication of this paper on the MUSCLES Treasury Survey Page on MAST: https://archive.stsci.edu/prepds/muscles/. Available products will include the standard data products provided by the MUSCLES survey (i.e., the SED at native and 1 Å resolutions along with the component observations and models), along with the new Semi-empirical model SED at native and 1 Å resolutions. The remainder of the Mega-MUSCLES targets, listed at http://cos.colorado.edu/~kevinf/muscles.html, will be added to the database in the coming months. Users with an interest in any particular target can contact the first author for an expedited production of that SED.

8. CONCLUSION

We have constructed a panchromatic SED of the M8 star TRAPPIST-1, the first data product from the Mega-MUSCLES survey.

The SED presented here represents the state-of-the-art for observation of the high-energy flux of low-mass stars, but also demonstrates the limits of our current observing capabilities. Obtaining the ultraviolet spectroscopy pushed COS to the limit of it's capabilities, with many predicted emission lines remaining below the noise limit. The EUV spectrum cannot be observed with any currently operating facility. Improving on these observations, which is desirable given the continued importance of low-mass stars in exoplanetology, will require the launch of large-aperture space telescopes with ultraviolet capabilities and/or a dedicated EUV observatory (Youngblood et al. 2019).

We thank S. Peacock for providing the PHOENIX EUV models. Based on observations made with the NASA/ESA Hubble Space Telescope, obtained from the Data Archive at the Space Telescope Science Institute, which is operated by the Association of Universities for Research in Astronomy, Inc., under NASA contract NAS 5-26555. These observations are associated with program # 15071. Support for program #15071 was provided by NASA through a grant from the Space Telescope Science Institute, which is operated by the Association of Universities for Research in Astronomy, Inc., under NASA contract NAS 5-26555. All of the HST data presented in this paper were obtained from the Mikulski Archive for Space Telescopes (MAST).

Facilities: HST (STIS and COS),

Software: astropy (Astropy Collaboration, 2013), stistools

APPENDIX

REFERENCES

Arnaud, K. A. 1996, in Astronomical Society of the Pacific Conference Series, Vol. 101, Astronomical Data Analysis Software and Systems V, ed. G. H. Jacoby & J. Barnes, 17

Astropy Collaboration, Robitaille, T. P., Tollerud, E. J., et al. 2013, A&A, 558, A33

Barstow, J. K., & Irwin, P. G. J. 2016, MNRAS, 461, L92

Bourrier, V., Ehrenreich, D., Wheatley, P. J., et al. 2017a, A&A, 599, L3

Bourrier, V., de Wit, J., Bolmont, E., et al. 2017b, AJ, 154, 121

Burgasser, A. J., & Mamajek, E. E. 2017, ApJ, 845, 110

de Wit, J., Wakeford, H. R., Gillon, M., et al. 2016, Nature, 537, 69

France, K., Loyd, R. O. P., Youngblood, A., et al. 2016, ApJ, 820, 89

Gillon, M., Jehin, E., Lederer, S. M., et al. 2016, Nature, 533, 221

Gillon, M., Triaud, A. H. M. J., Demory, B.-O., et al. 2017, Nature, 542, 456

Husser, T. O., Wende-von Berg, S., Dreizler, S., et al. 2013, A&A, 553, A6

Kopparapu, R. K., Ramirez, R. M., SchottelKotte, J., et al. 2014, ApJL, 787, L29

Linsky, J. L., Fontenla, J., & France, K. 2014, ApJ, 780, 61

Louden, T., Wheatley, P. J., & Briggs, K. 2017, MNRAS, 464, 2396

Loyd, R. O. P., France, K., Youngblood, A., et al. 2016, ApJ, 824, 102

Luger, R., Sestovic, M., Kruse, E., et al. 2017, Nature Astronomy, 1, 0129

O'Malley-James, J. T., & Kaltenegger, L. 2017, MNRAS, 469, L26

Peacock, S., Barman, T., Shkolnik, E. L., Hauschildt, P. H., & Baron, E. 2019, ApJ, 871, 235

Reiners, A., & Basri, G. 2009, ApJ, 705, 1416

Roettenbacher, R. M., & Kane, S. R. 2017, ApJ, 851, 77

Smith, R. K., Brickhouse, N. S., Liedahl, D. A., & Raymond, J. C. 2001, ApJ, 556, L91

Veras, D., Armstrong, D. J., Blake, J. A., et al. 2018, Astrobiology, 18, 1106

Vidal, C. R., Cooper, J., & Smith, E. W. 1973, 25, 37

Wang, S., Wu, D.-H., Barclay, T., & Laughlin, G. P. 2017, arXiv e-prints, arXiv:1704.04290

Wheatley, P. J., Louden, T., Bourrier, V., Ehrenreich, D., & Gillon, M. 2017, MNRAS, 465, L74

Woods, T. N., Chamberlin, P. C., Harder, J. W., et al. 2009, Geophys. Res. Lett., 36, L01101

Youngblood, A., France, K., Loyd, R. O. P., et al. 2016, ApJ, 824, 101

Youngblood, A., Drake, J., Mason, J., et al. 2019, BAAS, 51, 300